Vacancy distribution and ionic motion in LaF_3 studied by ^{19}F NMR

A. F. Aalders, A. F. M. Arts, and H. W. de Wijn
Fysisch Laboratorium, Rijksuniversiteit Utrecht, P. O. Box 80.000, 3508 TA Utrecht, The Netherlands
(Received 19 April 1985)

We report on ^{19}F pulse-NMR experiments on a single crystal of the fast ionic conductor LaF_3 from 100 to 1250 K. The spin-lattice relaxation time T_1 is measured at frequencies up to 140 MHz, and its counterpart in the rotating frame $T_{1\rho}$, in spin-locking fields up to 12 G. In the regime of composite free-induction decays two spin-spin relaxation times T_2 are extracted. The data are analyzed in terms of the equations of motion of the nuclear magnetizations on two fluorine sublattices, F_1 and $F_{2,3}$, with inclusion of fluorine-fluorine dipolar interactions and relaxation to paramagnetic impurities. To fit all data simultaneously, it appeared essential to assume an energy difference Q between the depth of the potential wells at the F_1 and $F_{2,3}$ sites in the sense that the anion vacancies preferentially populate the $F_{2,3}$ sublattice. The model then gives realistic values for the activation energies and attempt frequencies for jumps within and between the F_1 and $F_{2,3}$ sublattices, while $Q=0.119\pm0.005$ eV. Above 400 K, the vacancies occupy, with an increasing concentration, the F_1 positions, where the residence time is longer than on the $F_{2,3}$ sites. The model also accounts for the knee observed in the conductivity of LaF_3-structured materials versus reciprocal temperature on the basis of the defect-defect interaction between trapped F_1 vacancies and $F_{2,3}$ vacancies carrying the ionic conductivity.

I. INTRODUCTION

In the last two decades the solid electrolyte LaF_3 has been the subject of extensive experimental study because of its high fluorine ionic conductivity already at ambient temperatures. Whereas the motion of fluorine ions in systems with the fluorite structure, like BaF_2 and β-PbF_2,[1–3] is well understood, the mechanisms underlying the ionic conductivity in LaF_3 are still subject to debate. This is primarily due to the intricate, in comparison with that of fluorites, crystal structure of LaF_3. The latter has the so-called tysonite structure ($P\bar{3}C1$),[4] in which the fluorine ions occupy three distinct positions, F_1, F_2, and F_3, in the ratio 12:4:2. The sites F_2 and F_3 are, however, structurally equivalent to the extent that in studies of ionic motion, such as the one below, a simplified hexagonal $P6_3/mmc$ structure[5] may be adopted (Fig. 1).

A variety of techniques has been employed to investigate the ionic motion over the F_1 and combined $F_{2,3}$ sublattices in LaF_3. In the period 1965 to 1968 the first results were obtained by ^{19}F nuclear magnetic resonance (NMR), a technique capable of distinguishing between the sublattices. In a line-narrowing experiment performed by Lee and Sher[6] fast diffusive motion was found to occur on one sublattice only between 300 and 500 K. In addition, a small frequency shift between the resonances belonging to the two sublattices was observed. In similar studies by Lundin *et al.*,[7,8] it was concluded from the anisotropy of the shift that the faster moving ions are most probably those on the $F_{2,3}$ sublattice. In contradiction with this, ^{19}F pulse-NMR experiments of Goldman and Shen[9] pointed to a faster motion of the F_1 ions. Measurements by Shen[10] of the spin-spin relaxation times in LaF_3 doped with rare-earth fluorides PrF_3 and NdF_3 were consistent with the pulse-NMR results in pure LaF_3, and therefore the assignment of the faster motion to the F_1 sublattice was not critically reexamined. Further, thermal-expansion studies determined the intrinsic defect mechanism to be of the Schottky type, yet did not provide information that could solve the controversy as to the more mobile ions.[11]

Since 1977, interest in the ionic motion in LaF_3-structured ionic conductors has been renewed. Apart from studies on LaF_3 (Refs. 12–20) and CeF_3 (Refs. 21–23), this has resulted in a number of papers on the solid solutions $La_{1-x}Ba_xF_{3-x}$ (Refs. 12 and 24–28). A second controversy arose in the analysis of the bulk conductivity. At about 415 K the extrinsic conductivity of LaF_3 appears to exhibit a knee, at which the activation energy for thermal motion changes from about 0.45 eV

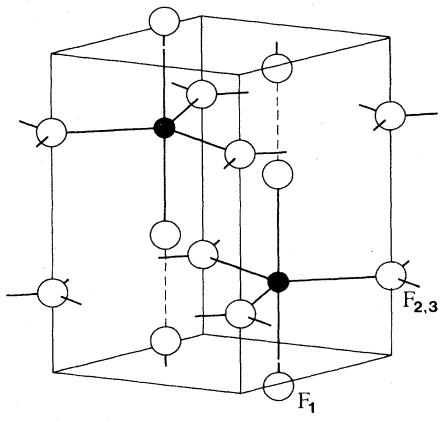

FIG. 1. Simplified crystal structure of LaF_3. The minute crystallographic distinction between the F_2 and F_3 positions is ignored.

below to approximately 0.26 eV above this temperature. This effect was initially ascribed to a changeover from an association-governed regime to a free-defect motion at higher temperatures.[13,15,20] Recent work, however, unambiguously demonstrated that such a transition cannot take place at 415 K on the grounds that the fluorine-ion vacancies are already completely dissociated at about 120 K.[12,28] This finding was fully confirmed by a comparison of the diffusion constants derived from the conductivity with those from NMR measurements.[25,26] Recently, a new theory has been proposed, which makes no use of the existence of dipolar complexes, but explains the knee in the conductivity on the basis of polarization effects induced by defect jumps between inequivalent sites.[29] The quantitative predictions of this model are however poor,[26] leaving doubt as to its applicability to LaF_3. Jaroszkiewicz and Strange[16] have performed an extensive study of the ^{19}F nuclear relaxation in LaF_3 in the temperature range 300—1000 K, including the spin-spin relaxation time T_2 as well as the spin-lattice relaxation times T_1 and $T_{1\rho}$ in the laboratory and rotating frames. These authors further succeeded in developing an inequivalent-site theory,[16,17] which is able to account for the observed complicated behavior of the relaxation times provided appropriate temperature dependences of the ionic jump frequencies are inserted. Despite the inherent power of their theory, at best qualitative results were obtained. In particular, as we will see below, the assumptions made in regard to the activation energies of the various jumps led to unrealistic results. Furthermore, the effects of paramagnetic rare-earth impurities, which in any real specimen LaF_3 are unavoidably present, were ignored.

In this paper we report on NMR relaxation-time measurements of T_1, $T_{1\rho}$, and T_2 in LaF_3 at temperatures ranging from 100 to 1250 K and over a wide range of frequencies. To arrive at a complete analysis, the model of Jaroszkiewicz and Strange is extended to include the effects of nuclear spin relaxation induced by paramagnetic impurities. This is accomplished on the basis of the continuum-diffusion theory developed by Rorschach[30] and Richards[31] upon taking into account the substantial difference between the fluorine diffusion on the F_1 and $F_{2,3}$ sublattices. Further, it appeared essential to assume that the potential well for fluorine ions differs in depth on the F_1 sites and on the $F_{2,3}$ sites. This difference, of structural rather than defect-chemical origin, induces a distribution of the vacancies over the sublattices, such that at low temperatures the vacancies preferentially reside on the $F_{2,3}$ sites, where they exhibit fast motion. It is finally argued that the redistribution of the vacancies at higher temperatures produces the knee observed in the conductivity.

II. EXPERIMENTAL RESULTS

The ^{19}F spin-relaxation times T_1, T_2, and $T_{1\rho}$ were measured in the frequency range 20—140 MHz, using a pulse-NMR spectrometer built of standard components. Phase-sensitive detection with reference to the oscillator frequency was employed. T_1 was obtained from the intensity of the free-induction decay following a 90°-τ-90° pulse sequence. For long T_1's this sequence was preceded by a saturating comb of 90° pulses, allowing a faster repetition rate. At low temperatures, T_2 was deduced from the free-induction decays, and at high temperatures from a 90°-τ-180° spin-echo technique. $T_{1\rho}$ was measured with a 90° pulse, followed by a spin-locking pulse of length τ having an rf phase shifted by 90° with reference to the first pulse. The corresponding spin-locking fields H_1 were varied from 5 to 12 G. The maximum measurable $T_{1\rho}$ was set by the maximum pulse length provided by the rf amplifier (Matec 525), which was typically a few milliseconds. All pulse sequences were generated with a microcomputer system. The decay and spin-echo signals were stored in a Biomation 8100 fast digitizer, and fed to the microcomputer for efficient signal averaging and data reduction.

The single crystals of lanthanum fluoride was grown from the melt by a modified Stockbarger method using rf-induction heating.[32] The samples were of cylindrical form, typically 8 mm in diameter and 10 mm long. For NMR above room temperature, the crystals were sealed in quartz ampoules under a He-gas atmosphere, which resulted in excellent reproducibility in thermal cycling, even above 1000 K. The rf coil, made of gold wire, was wound on the outer surface of the ampoule. The whole assembly was mounted in an oven capable of reaching temperatures up to 1250 K and placed between the pole caps of a standard Fe-yoke NMR magnet. The sample could be rotated *in situ* about an axis perpendicular to the magnetic field. Below 330 K, a number of experiments were carried out in a superconducting magnet, enabling us to extend the frequency range to 140 MHz. In the latter case the coil was wound directly around the sample.

In Fig. 2 we present the data for the relaxation times. The dependences of T_1 on temperature and frequency are quite complex. According to the physical processes that play a role, three regimes can be distinguished. Below 250 K, T_1 is virtually constant and about proportional to $\omega_0^{0.4}$, where ω_0 is the angular Larmor frequency. The constant T_1 of order 10 s points to relaxation by magnetic impurities, i.e., T_1 is determined by the temperature-independent rate associated with spin diffusion towards the paramagnetic centers. We note, however, that the T_1's reported here are among the longest reported in the literature, reflecting the purity of the sample. In the second regime, from 250 to 500 K, ionic diffusion sets in, increasing the rate of transport. T_1 decreases, and is nearly frequency independent. In a $\log_{10}T_1$ vs $1/T$ plot, such as in Fig. 2, the decrease is described by a slope $\Delta E = 0.33 \pm 0.02$ eV. This equals within errors the $\Delta E = 0.29 \pm 0.05$ eV found in LaF_3 doped with Nd^{3+} to concentrations of 0.1 mole %,[10] reflecting the fact that paramagnetic impurities are still involved. Above 500 K, ΔE diminishes until T_1 reaches its minimum at 1000 K. Concurrently, the frequency dependence becomes stronger. Here paramagnetic relaxation is eclipsed by spin-lattice relaxation invoked by the motion modulation of the ^{19}F dipolar interaction. Although above 1000 K only a few data points are available, T_1 is seen to increase sharply with temperature upon merging with T_2 and $T_{1\rho}$.

The spin-spin relaxation time T_2 exhibits a temperature

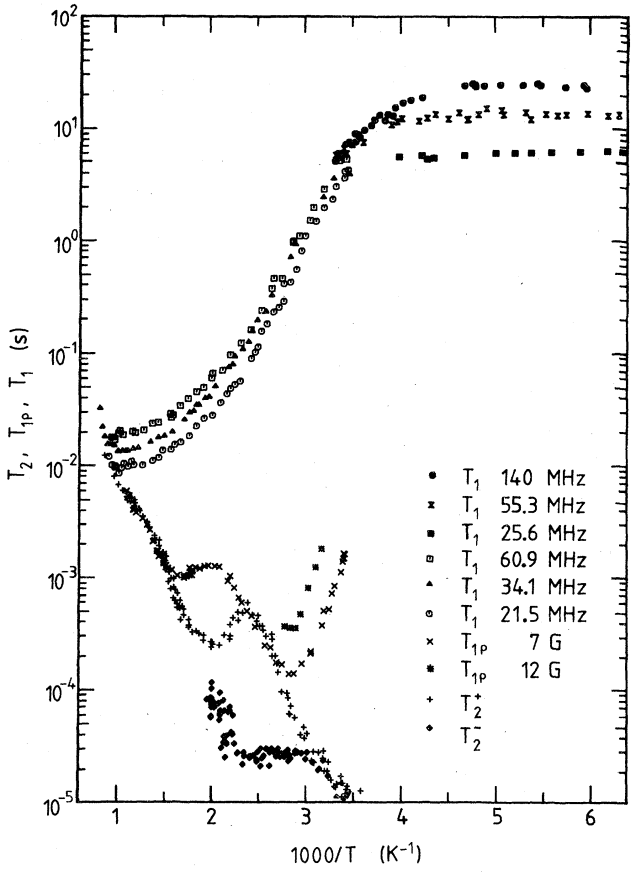

FIG. 2. Relaxation times T_2, $T_{1\rho}$, and T_1 vs the reciprocal temperature in LaF_3 under the conditions as indicated. Experimental errors of the relaxation times typically are 10%.

dependence that is characteristic for tysonite-structured ionic conductors, and has previously been observed by several authors.[9,10,15,16,22] As first noticed by Goldman and Shen,[9] the free-induction decay is composite between 320 and 570 K. Two decays can be discerned. Quite essential to the analysis below is that, in the present experiments, the time constants of both components of the free-induction decay could be tracked over a wide range of temperatures. Further, the two decays are found to differ slightly in the angular dependence of their resonance conditions, which directly proves that the decays belong to ^{19}F nuclei on different sites. This was conjectured earlier to be the case from line-shape studies.[6–8] For $\mathbf{H}_0||c$ axis, a beat structure is observed in the short decay when the long decay is maintained at resonance (upper trace of Fig. 3). The beat frequency cannot be determined to great accuracy because of the shortness of the decay, but is of order 10 kHz. It reduces with increasing temperature, and vanishes when the free-induction decays change to single exponential functions. For $\mathbf{H}_0\perp c$ axis, on the other hand, no beats are observed at any temperature (lower trace of Fig. 3). This direction of the field was therefore applied when measuring T_2, but we note that the few data obtained with $\mathbf{H}_0||c$ axis show no marked deviations. As to the temperature dependence of the T_2's, the longer one increases with $\Delta E \approx 0.45$ eV when going from room temperature to 415 K, while the shorter T_2, about 25 μs, stays constant. Above 415 K, the longer T_2 decreases, reaching a minimum at about 500 K, whereas the shorter T_2 exhibits motional narrowing with $\Delta E \approx 0.5$ eV. Above 550 K a single T_2 remains, which increases with increasing temperature. The rise does not, however, have a unique ΔE. Two additional kinks are observed, one at $T \approx 700$ K to a somewhat smaller ΔE, and a second one above 1000 K to a very steep slope $\Delta E \approx 0.85$ eV.

The $T_{1\rho}$ data (Fig. 2) show two minima, which shift towards higher temperatures with increasing locking fields. Below 360 K, where $T_{1\rho}$ is minimum, $T_{1\rho}$ is proportional to ω_1^2, with $\omega_1 = g_F \mu_N H_1/\hbar$, suggesting a Bloembergen-Purcell-Pound (BPP) behavior (Fig. 4). In this region ΔE corresponds to an activation energy of 0.47 ± 0.02 eV, in excellent accord with the result from $T_{1\rho}$ reported by Ildstad *et al.*,[14] 0.48 ± 0.04 eV. From 360 K up to 415 K,

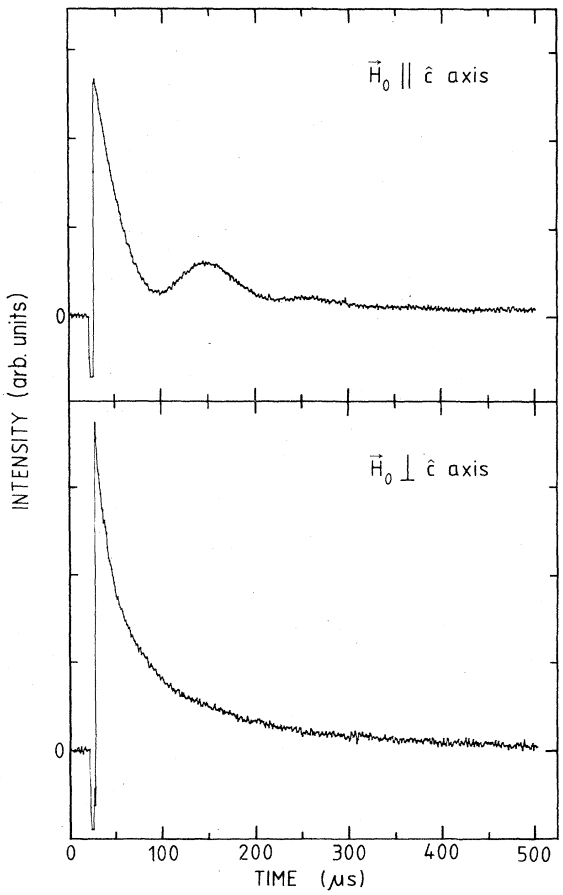

FIG. 3. Free-induction decays for LaF_3 at 430 K for $\mathbf{H}_0||c$ axis (upper trace) and $\mathbf{H}_0\perp c$ axis (lower trace). The decays are of composite nature ($T_2^- \approx 25$ μs, $T_2^+ \approx 350$ μs) due to the difference in fluorine mobility on the two sublattices. For $\mathbf{H}_0\perp c$ axis, the F_1 and $F_{2,3}$ resonances coincide; for $\mathbf{H}_0||c$ axis, the F_1 resonance is shifted, producing beats with the oscillator tuned to $F_{2,3}$.

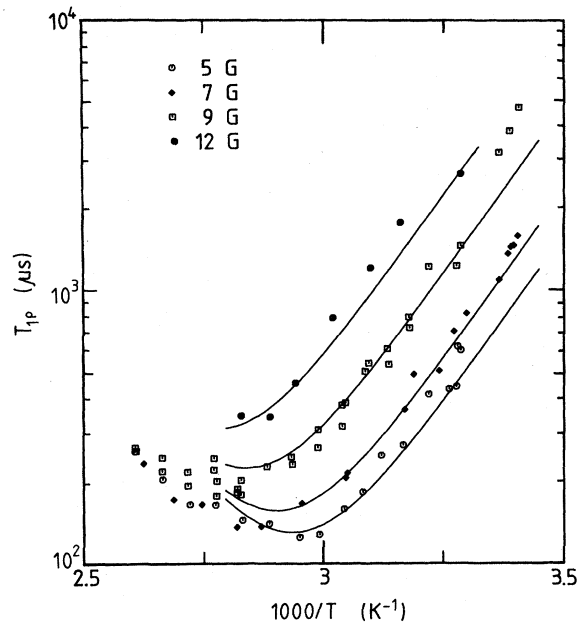

FIG. 4. Spin-lattice relaxation time in the rotating frame, $T_{1\rho}$, vs the inverse temperature in the regime where $\omega_1 > \Gamma$. Curves represent the BPP behavior $T_{1\rho}^{-1} = W\Gamma/(\omega_1^2+\Gamma^2)$, where $\Gamma = \Gamma^{\infty}\exp(-\Delta E/kT)$.

$T_{1\rho}$ equals T_2. Unlike T_2, $T_{1\rho}$ continues to rise above 415 K until a weak decrease sets in at 500 K. The second minimum is observed at 570 K, weakly dependent on ω_1. $T_{1\rho}$ again becomes equal to T_2 above 600 K, and eventually concurs with T_1 at 1000 K.

III. NUCLEAR RELAXATION IN LaF_3

A. Two-sublattice model

We consider two sublattices, α and β, which, apart from being distinct crystallographically, are in different thermal motion. In LaF_3 the ionic conductivity is brought about by the motion of fluorine vacancies, and the intrinsic point defects are of the Schottky type.[11,33] The inverse lifetime for a particular ion to stay on a certain position depends on the sublattice, and is for the α sublattice given by

$$\tilde{\Gamma}_{\alpha} = \Gamma_{\alpha\alpha} + \Gamma_{\alpha\beta} , \tag{1}$$

and similarly $\tilde{\Gamma}_{\beta}$ for the β sublattice. Here, $\Gamma_{\alpha\alpha}$ is the jump rate from one α to another α position integrated over all possible α-α jumps, and $\Gamma_{\alpha\beta}$ similarly is the jump rate from an α site to the β sublattice. We assume the α sublattice to be the faster one at room temperature. The equations of motion of the nuclear magnetizations on the α and β sublattice are coupled by virtue of the dipolar interaction. Jaroszkiewicz and Strange[17] have already worked out these equations for the longitudinal magnetization M_z as well as the transverse magnetizations M_x and M_ρ in the laboratory and rotating frames. Their analysis included, in addition to the dipolar interaction between the ^{19}F nuclei, the interaction of the ^{19}F with the ^{139}La nuclei ($S=\frac{7}{2}$, $g_{La}=0.789$), which are assumed to stay in thermal equilibrium with the lattice.

Omitting the Larmor-frequency part of the equations of motion, one has for the longitudinal component of the magnetization residing on the α sublattice[17]

$$\begin{aligned}\frac{d}{dt}\langle M_z^{\alpha}\rangle = -\Bigg[&\frac{K^2}{16}\{18J_{\alpha\alpha}^{(1)}(\omega_F)+18J_{\alpha\alpha}^{(2)}(2\omega_F)+J_{\alpha\beta}^{(0)}(0)+18J_{\alpha\beta}^{(1)}(\omega_F)\\ &+9J_{\alpha\beta}^{(2)}(2\omega_F)+\tfrac{4}{3}S(S+1)(g_{La}/g_F)^2[J_{\alpha,La}^{(0)}(\omega_F-\omega_{La})+18J_{\alpha,La}^{(1)}(\omega_F)+9J_{\alpha,La}^{(2)}(\omega_F+\omega_{La})]\}+\Gamma_{\alpha\beta}\Bigg]\langle M_z^{\alpha}\rangle\\ -\Bigg[&\frac{K^2}{16}\frac{N^{\alpha}}{N^{\beta}}[9J_{\alpha\beta}^{(2)}(2\omega_F)-J_{\alpha\beta}^{(0)}(0)]-\Gamma_{\beta\alpha}\Bigg]\langle M_z^{\beta}\rangle ,\end{aligned} \tag{2}$$

and for the rotating-frame component

$$\begin{aligned}\frac{d}{dt}\langle M_\rho^{\alpha}\rangle = -\Bigg[&\frac{K^2}{32}\{9J_{\alpha\alpha}^{(0)}(2\omega_1)+90J_{\alpha\alpha}^{(1)}(\omega_F)+9J_{\alpha\alpha}^{(2)}(2\omega_F)+\tfrac{1}{2}J_{\alpha\beta}^{(0)}(0)\\ &+\tfrac{9}{2}J_{\alpha\beta}^{(0)}(2\omega_1)+54J_{\alpha\beta}^{(1)}(\omega_F)+9J_{\alpha\beta}^{(2)}(2\omega_F)\\ &+\tfrac{4}{3}S(S+1)(g_{La}/g_F)^2[J_{\alpha,La}^{(0)}(\omega_F-\omega_{La})+4J_{\alpha,La}^{(0)}(\omega_1)+18J_{\alpha,La}^{(1)}(\omega_F)\\ &+18J_{\alpha,La}^{(1)}(\omega_{La}+\omega_1)+18J_{\alpha,La}^{(1)}(\omega_{La}-\omega_1)+9J_{\alpha,La}^{(2)}(\omega_F+\omega_{La})]\}+\Gamma_{\alpha\beta}\Bigg]\langle M_\rho^{\alpha}\rangle\\ -\Bigg[&\frac{K^2}{32}\frac{N^{\alpha}}{N^{\beta}}[-\tfrac{1}{2}J_{\alpha\beta}^{(0)}(0)+\tfrac{9}{2}J_{\alpha\beta}^{(0)}(2\omega_1)+36J_{\alpha\beta}^{(1)}(\omega_F)]-\Gamma_{\beta\alpha}\Bigg]\langle M_\rho^{\beta}\rangle ,\end{aligned} \tag{3}$$

and similarly for $\langle M_z^\beta \rangle$ and $\langle M_\rho^\beta \rangle$. The equations of motion of the transverse magnetization $\langle M_x^{\alpha,\beta} \rangle$ follow from Eq. (3) by setting $\omega_1 = 0$. Here, ω_F and ω_{La} are the angular frequencies of the fluorine and lanthanum nuclei, g_F and g_{La} are the corresponding nuclear g factors, and N^α and N^β are the numbers of α and β sites. Furthermore,

$$K = (\mu_0/4\pi\hbar)(\mu_N g_F)^2 .$$

The functions $J_{ij}^{(q)}(\omega)$ ($q = 0,1,2$) are the standard Fourier transforms of the spatial-correlation functions of the dipolar interaction summed over the sublattice j, the subscripts referring to the fluorine and lanthanum sublattices in an obvious notation. The equations for $\langle M_z^\alpha \rangle$ and $\langle M_z^\beta \rangle$ as well as those for the ρ and x components of the magnetizations are coupled, and of the general form

$$\frac{d}{dt}\langle M^\alpha \rangle = a_{11}\langle M^\alpha \rangle + a_{12}\langle M^\beta \rangle ,$$
$$\frac{d}{dt}\langle M^\beta \rangle = a_{21}\langle M^\alpha \rangle + a_{22}\langle M^\beta \rangle , \tag{4}$$

implying that the spin system will return to equilibrium, $\langle M_z^{\alpha,\beta} \rangle_{eq} = M_0$, $\langle M_\rho^{\alpha,\beta} \rangle_{eq} \approx 0$, and $\langle M_x^{\alpha,\beta} \rangle_{eq} = 0$, with relaxation rates

$$\frac{1}{T_k^\pm} = -\tfrac{1}{2}\{(a_{11}+a_{22}) \pm [(a_{11}-a_{22})^2 + 4a_{12}a_{21}]^{1/2}\} , \tag{5}$$

where the index k denotes 1, 1ρ, and 2, referring to the longitudinal, rotating-frame, and transverse magnetizations, respectively. We have $T_k^+ \geq T_k^-$.

It is of interest at this point to examine, as a function of the temperature, the general characteristics of the decay predicted by the above equations. As has been noted above, in the actual experiments one essentially measures the decay of the total magnetization $\langle M^\alpha + M^\beta \rangle$. This sum, like $\langle M^\alpha \rangle$ and $\langle M^\beta \rangle$ by themselves, is not necessarily an eigenfunction of Eq. (4). The relaxation is accordingly of composite nature, i.e., a linear combination, determined by the initial conditions, of the exponential decays with time constants $T_k^\pm$. In the free-induction decays, probing $\langle M_x^\alpha + M_x^\beta \rangle$, a double-exponential decay is indeed observed between 320 and 550 K. At higher temperatures, the exchange of ions between the sublattices has become fast to the extent that the rates $\Gamma_{\alpha\beta}$ and $\Gamma_{\beta\alpha}$ are the dominant terms of Eq. (4). Under this condition, as is borne out by a detailed inspection of the equations of motion, $\langle M_x^\alpha + M_x^\beta \rangle$ is a good eigenfunction, leading to single-exponential free-induction decays. Contrary to $\langle M_x^\alpha + M_x^\beta \rangle$, $\langle M_z^\alpha + M_z^\beta \rangle$ appears to decay in single-exponential form over the entire temperature range considered. In this case, even when the exchange of ions between the sublattices is slow, fast equilibrium of the magnetization between the α and β sublattices is provided by the dipolar coupling terms $J_{\alpha\beta}^{(0)}(0)$ [cf. Eq. (2)]. The same reasoning applies, although to a lesser degree, to the relaxation of $\langle M_\rho^\alpha + M_\rho^\beta \rangle$. The effect of $J_{\alpha\beta}^{(0)}(0)$ is smaller here by a factor of 4 owing to the smaller prefactor in Eq. (3), and further weakened by a substantial contribution of $J_{\alpha\alpha}^{(0)}(2\omega_1)$. In the course of the present experiments, a double exponential $T_{1\rho}$ was indeed observed in the range, where both components of the free-induction decays are motionally narrowed. Although the shorter time constant could not be accurately determined, it was estimated of the order of T_2^-.

TABLE I. Powder-averaged rigid-lattice second moments W_{ij} for LaF_3. All W_{ij} are in rad^2/s^2. The subscripts $i,j = 1,2$, and La denote F_1, $F_{2,3}$, and La sites, respectively.

	$j=1$	$j=2$	$j=$La
$i=1$	3.27×10^9	2.11×10^9	5.99×10^8
$i=2$	4.22×10^9	5.43×10^8	7.64×10^8

In the calculation of the relaxation times below, the spectral densities $J_{ij}^{(q)}(\omega)$, have to be expressed in terms of the hopping frequencies $\Gamma_{\alpha\alpha}$, $\Gamma_{\beta\beta}$, and $\Gamma_{\alpha\beta}$. The simplest approach is based on an exponential decay of the correlation functions. This leads to the well-known BPP expressions for the spectral densities

$$J_{ij}^{(q)}(\omega) = \frac{4}{15}\frac{C^{(q)}(\tilde{\Gamma}_i + \tilde{\Gamma}_j)}{\omega^2 + (\tilde{\Gamma}_i + \tilde{\Gamma}_j)^2}\sum_{j(\neq i)}\frac{1}{r_{ij}^6} , \tag{6}$$

where $C^{(0)}$, $C^{(1)}$, and $C^{(2)}$ equal 6, 1, and 4, respectively. The summations are related to the rigid-lattice second moments

$$W_{ij} = \tfrac{3}{5}K^2 I(I+1)\sum_{j(\neq i)} r_{ij}^{-6} ,$$

in which j runs over the sites of a sublattice, while i is fixed. Values for the relevant W_{ij} are given in Table I. More elaborate expressions for $J_{ij}^{(q)}(\omega)$ have been derived in the case of diffusion on simple lattices,[34] inclusion of which makes the minima of T_1 and $T_{1\rho}$ as a function of the inverse temperature slightly asymmetric and further affects the dependence of $T_{1\rho}$ on the field orientation. The latter approach is not simply applicable to the ^{19}F sublattices in LaF_3, but a comparison with the BPP results in the case of BaF_2, in which the ^{19}F form a simple-cubic lattice, leads one to believe that Eq. (6) is adequate. Although the angular dependence of $T_{1\rho}$ in BaF_2 is better described by the extended theory,[35] the temperature dependence at a fixed angle is equally well accounted for by simple exponentially decaying correlations. At low temperatures the dipolar fluctuations of the static lattice prevail. The fastest time of equilabration of the two sublattices by dipolar processes is then given by approximately the inverse rigid-lattice linewidth. In Eq. (6), this is incorporated by replacing $\tilde{\Gamma}_i + \tilde{\Gamma}_j$ by $W_{ij}^{1/2}$ when $\tilde{\Gamma}_i + \tilde{\Gamma}_j < W_{ij}^{1/2}$. At high temperatures, the sublattices reach mutual equilibrium by rapid exchange of ions, which is expressed by the $\Gamma_{\alpha\beta}$ in Eqs. (2) and (3).

B. Relaxation by paramagnetic impurities

Paramagnetic impurities, even in the smallest concentrations, have appreciable effects on the ^{19}F nuclear relaxation in LaF_3, in particular the spin-lattice relaxation. (Commercially available LaF_3 typically contains several

hundred ppm of the magnetic lanthanides.) T_1 is dominated by these impurities up to, say, 500 K. Effects on T_2 and $T_{1\rho}$ are only expected in the regime of strong motional narrowing, i.e., at high temperatures. The dominant interaction between the fluorine nuclear spins and the rare-earth electronic spins is dipolar, rather than transferred hyperfine as in the case of $3d$ transition-metal impurities.[36] The problem of nuclear spin-lattice relaxation by paramagnetic impurities has been treated extensively in the literature. Here, we follow the approach of Richards,[31] which combines classical spin and particle diffusion in a continuum representing a lattice of equivalent sites. We only indicate the basic assumptions of the theory, as necessary for extension to a ionic conductor containing inequivalent sites.

In the continuum theory, the time dependence of $\langle M_z \rangle$ in the presence of a single paramagnetic impurity is given by the diffusion equation

$$\frac{d(\langle M_z \rangle - M_0)}{dt} = D\nabla^2(\langle M_z \rangle - M_0) - \frac{C}{r^6}(\langle M_z \rangle - M_0) , \tag{7}$$

where D is the diffusion coefficient of the nuclear spins, and

$$C = \tfrac{2}{5} K K_p S_p (S_p + 1)\tau_p / [1 + (\omega_F \tau_p)^2] \tag{8}$$

represents the dipolar interaction of the nuclear spin with the impurity electronic spin $\mathbf{S}_p$. In Eq. (8), τ_p is the correlation time of the z component of $\mathbf{S}_p$, and

$$K_p = (\mu_0 / 4\pi\hbar)(\mu_B g_p)^2 .$$

The mechanisms contributing to the transport of nuclear magnetization towards the impurity are ionic diffusion and spin diffusion. In the event the ionic diffusion is fast, such as at high temperatures, C has to be replaced by C', which differs from C in that

$$\tau_p' = (1/\tau_p + \tilde{\Gamma})^{-1} \tag{9}$$

substitutes for τ_p. Equation (9) reflects that in the case of fast ionic diffusion it is the inverse ionic hopping frequency rather than the correlation time of the electronic spin that determines the time scale of the impurity-invoked fluctuating fields at the ^{19}F nuclei. The two diffusion processes differ in their dependence on distance. Spin diffusion is quenched when the local magnetic field varies strongly from site to site, i.e., in the present case within a radius

$$b = (3\langle \mu_p \rangle / \mu_F)^{1/4} a_{\text{La-La}} \tag{10}$$

about the impurity, dependent on the temperature and the external magnetic field through the effective impurity moment $\langle \mu_p \rangle$ that is static during T_2;[30] μ_F is the fluorine nuclear magnetic moment, and $a_{\text{La-La}}$ the nearest-neighbor La-La separation. Ionic diffusion is not limited by this barrier, but can take the energy up to the distance of closest approach $a_{\text{La-F}}$, the nearest-neighbor La-F distance. Thus, the diffusion constant D will change from $D_S + D_i$ for $r > b$ to D_i for $a_{\text{La-F}} < r < b$, with

$$D_i = \tfrac{1}{6} f a_{\text{F-F}}^2 \tilde{\Gamma}, \quad D_S = \tfrac{1}{6} f a_{\text{F-F}}^2 / T_2 . \tag{11}$$

Here, $a_{\text{F-F}}$ is the F-F distance, and f is the correlation factor for successive jumps, which is $\frac{2}{3}$ in the LaF_3 structure.[28] In the temperature regime, where D_S is dominant, T_2 can safely be approximated by T_{20}, the spin-spin relaxation time of the rigid lattice.

When solving Eq. (7) with the appropriate boundary conditions at b and $a_{\text{La-F}}$, the impurity-induced relaxation rate is found to read[31]

$$\frac{1}{T_1^{(p)}} = 8\pi N_p C^{1/4} (D_i + D_S)^{3/4} \frac{\Gamma(3/4)}{\Gamma(1/4)} \left[\frac{q_0 I_{3/4}(\delta) - I_{-1/4}(\delta)}{q_0 I_{-3/4}(\delta) - I_{1/4}(\delta)} \right] , \tag{12}$$

where N_p is the impurity concentration, and

$$q_0 = \left[\frac{C(D_i + D_S)}{C' D_i} \right]^{1/2} \left[\frac{I_{-1/4}(\delta') I_{-3/4}(\delta_a) - I_{3/4}(\delta_a) I_{1/4}(\delta')}{I_{3/4}(\delta') I_{-3/4}(\delta_a) - I_{3/4}(\delta_a) I_{-3/4}(\delta')} \right] . \tag{13}$$

The I are modified Bessel functions, while $\delta = [C/(D_i + D_S)]^{1/2}/2b^2$, $\delta' = (C'/D_i)^{1/2}/2b^2$, and $\delta_a = (C'/D_i)^{1/2}/2a_{\text{La-F}}^2$. In the limits $D_i \gg D_S$ and $D_i \ll D_S$, Eq. (12) reduces to simpler expressions, for which one is referred to Ref. 31.

Equation (12) essentially expresses the spin-lattice relaxation of equivalent spins by diffusion over equivalent sites. In applying Eq. (12) to the present problem one should note, of course, that this rate differs for the two sublattices [cf. Eqs. (1), (9), and (11)], forcing one to discern $T_{1,\alpha}^{(p)}$ and $T_{1,\beta}^{(p)}$, with a corresponding distinction in the diffusion constant D_i, and strictly speaking, D_S. Solving Eqs. (4) with the right-hand side of Eq. (7) included would be prohibitively difficult. The relaxation by the paramagnetic impurities may, however, heuristically be added to the result of Eqs. (5) above by accounting for the associated rates by the substitutions $a_{11} \to a_{11} - 1/T_{1,\alpha}^{(p)}$ and $a_{22} \to a_{22} - 1/T_{1,\beta}^{(p)}$. Note that this procedure does not introduce any new time constants in the decays of the various components of the magnetization, but simply modifies the ones of Sec. III A to become

$$\frac{1}{T_k^{\pm}} = -\frac{1}{2}\left\{\left[a_{11}-\frac{1}{T_{1,\alpha}^{(p)}}+a_{22}-\frac{1}{T_{1,\beta}^{(p)}}\right] \pm \left[\left[a_{11}-\frac{1}{T_{1,\alpha}^{(p)}}-a_{22}+\frac{1}{T_{1,\beta}^{(p)}}\right]^2 + 4a_{12}a_{21}\right]^{1/2}\right\}. \quad (14)$$

Note that, on the time scale of T_1, the sizable off-diagonal elements in Eqs. (2) still maintain a single spin temperature on the two sublattices at all temperatures. In the case of LaF_3 below 500 K, the contributions by magnetic impurities originate almost exclusively from $1/T_{1,\alpha}^{(p)}$. At higher temperatures, the diffusion on the α sublattice becomes fast to the degree that the associated relaxation ceases to be effective [cf. Eq. (9)]. At these temperatures, however, the slower diffusion on the β sublattice takes over.

IV. INTERPRETATION

A. Defect motion

In Sec. III we have distinguished two sublattices, the fast α and slow β, without indicating explicitly which ionic positions, F_1 or $F_{2,3}$, they refer to. As it turns out, the most decisive experimental material in the identification of the sublattice carrying the faster moving ions is the composite T_2 versus temperature. In the expression for the noncomposite $T_{1\rho}$ interchanging F_1 and $F_{2,3}$ leads to fits of equal quality by a suitable adjustment of the jump frequencies Γ. As regards T_2, rigid-lattice summation over both sublattices yields $T_2=13$ μs, which indeed is the value observed below 300 K (Fig. 2). As already pointed out, the two components of the free-induction decay become distinct above 320 K, where the one with the longer time constant, T_2^+, exhibits activated behavior, whereas the shorter T_2^- stays virtually constant at a level of about 25 μs up to 415 K. In the range 320–415 K, T_2^+ increases by an order of magnitude. Evidently, T_2^- is primarily determined by the rigid sublattice, and not very much affected by the thermal motion of the other sublattice. Upon keeping the $F_{2,3}$ sublattice rigid, and incorporating the motion of the F_1 sublattice in the way discussed below, the theory of Sec. III predicts $T_2^- \approx 60$ μs, as opposed to $T_2^- \approx 20$ μs for the reverse situation of a rigid F_1 sublattice and a $F_{2,3}$ sublattice in thermal motion, the difference reflecting W_{22} in relation to W_{11}. Therefore, the obvious conclusion, which is confirmed by the complete analysis in Sec. IV B, is that the ions on the $F_{2,3}$ sublattice are the faster ones. We accordingly make the assignments $\alpha=F_{2,3}$ and $\beta=F_1$, implying a ratio of the number of fast-moving ions over the number of slow-moving ions of $N^\alpha/N^\beta=\frac{1}{2}$. Further experimental evidence for fast $F_{2,3}$ motion is found in Fig. 3, where the composite decay displays a beat structure of the component with the shorter time constant, which is as already noted above, associated with the slower ions. The anisotropy of this beat with the orientation of the external field is evidence for the presence of covalent bonding in the chemical shifts. Indeed, this bonding is strongest for the F_1 ions.[7,8] These very direct findings from NMR are in conformity with the results of a recent examination of the conductivity in single crystals of LaF_3.[12,26] The conductivity was found to be anisotropic up to 415 K, with the conductivity the largest along the c axis. Another property affected by the bulk conductivity, the dielectric relaxation, shows a similar behavior between 150 and 200 K.[28] The explanation here is that only the $F_{2,3}$ ions can form an uninterrupted conduction path along the c axis. Large vibrational amplitudes of the $F_{2,3}$ ions in the direction of the c axis, reflecting the formation of these paths, were indeed observed by x-ray and neutron diffraction measurements.[18]

In the extrinsic regime, which extends up to 715 K,[12,26] the fluorine vacancies, responsible for the ionic conductivity, are introduced by the inevitable presence of oxygen, whereas above 715 K the intrinsic generation of vacancies by the Schottky mechanism becomes manifest. A strictly random distribution of vacancies in the lattice would result in equal concentrations of vacancies on the two sublattices, or $[V_\alpha]=[V_\beta]$, in the defect notation of Kröger.[37] There are however no *a priori* reasons to assume this condition to hold for systems with inequivalent sites, i.e., the depth of the potential wells for the mobile ions are sublattice dependent (Fig. 5). In the case of LaF_3, if Q is the energy difference between inequivalent sites, the vacancies will be distributed according to a Boltzmann factor,

$$\frac{[V_\beta]}{[V_\alpha]} = \frac{[V_1]}{[V_{2,3}]} = e^{-Q/kT}. \quad (15)$$

The quantity Q appears to be an important parameter in our problem, as it has strong effects on the exchange rates of vacancies between the α and β sublattice. The exchange rates $\Gamma_{\alpha\beta}$ and $\Gamma_{\beta\alpha}$ are coupled by detailed balance. That is

$$(1-[V_\alpha])N^\alpha\Gamma_{\alpha\beta}=(1-[V_\beta])N^\beta\Gamma_{\beta\alpha}, \quad (16)$$

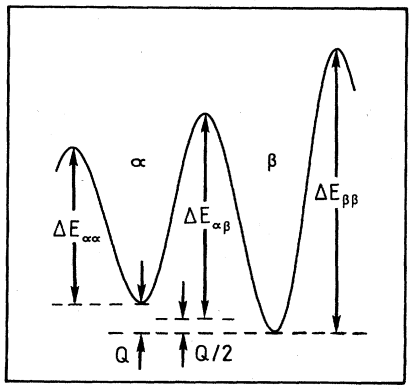

FIG. 5. Schematic representation of the energy barriers of the ionic jumps, with the activation energies indicated. The depth of the potential wells at the α and β sublattices differ by Q.

which in case $N^{\alpha}[V_{\alpha}^{\cdot}]+N^{\beta}[V_{\beta}^{\cdot}] \ll N=N^{\alpha}+N^{\beta}$, appropriate to our system in the extrinsic regime below ~ 715 K, reduces to $\Gamma_{\alpha\beta}/\Gamma_{\beta\alpha}=N^{\beta}/N^{\alpha}$.

We will adopt the usual single-activation-energy form for the jump frequencies of the individual ions, with inclusion of the probability of finding a nearest-neighbor vacancy,

$$\Gamma_{\alpha\alpha}(T)=[V_{\alpha}^{\cdot}]\Gamma_{\alpha\alpha}^{\infty}e^{-\Delta E_{\alpha\alpha}/kT}, \tag{17}$$

where $\Delta E_{\alpha\alpha}$ is the migration energy for hopping among α sites, and $\Gamma_{\alpha\alpha}^{\infty}$ denotes the "attempt" frequency. Similarly (cf. Fig. 5),

$$\begin{aligned}\Gamma_{\alpha\beta}(T)&=[V_{\beta}^{\cdot}]\Gamma_{\alpha\beta}^{\infty}e^{-(\Delta E_{\alpha\beta}-Q/2)/kT},\\ \Gamma_{\beta\alpha}(T)&=[V_{\alpha}^{\cdot}]\Gamma_{\beta\alpha}^{\infty}e^{-(\Delta E_{\alpha\beta}+Q/2)kT},\end{aligned} \tag{18}$$

where the choice $\Gamma_{\alpha\beta}^{\infty}/\Gamma_{\beta\alpha}^{\infty}=N^{\beta}/N^{\alpha}$ is necessary to fulfill detailed balance. It is noted that in the extrinsic regime the total concentration of vacancies, $[V^{\cdot}]$, is for our specimen known from an independent source, viz., experiments on the dielectric relaxation.[28] We have

$$[V^{\cdot}]=(N^{\alpha}[V_{\alpha}^{\cdot}]+N^{\beta}[V_{\beta}^{\cdot}])/N=6\times 10^{-4}.$$

B. Fitting of parameters

Insertion of the jump frequencies in the spectral densities, Eq. (6), yields expressions for T_2, $T_{1\rho}$, and T_1, Eq. (14), which depend on the temperature in a complicated manner, especially above 400 K, where motional narrowing, particle exchange, and diffusion to paramagnetic impurities all contribute to the relaxation. These expressions were least-squares fitted to a representative selection of 162 data points. The selection consisted of 60 T_2, 42 $T_{1\rho}$, and 60 T_1 points, and was made to cover a wide range of temperatures and frequencies. Although both T_2 components were observed in the decays, the longer one (T_2^{+}) could be extracted to much better accuracy than the faster one (T_2^{-}). Therefore, only the T_2^{+} were included in the adjustments. Above 400 K only spin-echo values of T_2^{+} were taken. For $T_{1\rho}$, a series with $H_1=\omega_1/\gamma_F=7$ G extending from 300 up to 900 K was chosen. The T_1 data consisted of four series, two from 130 to 300 K at 25.6 and 140.0 MHz, and two from 300 to 1050 K at 21.5 and 60.9 MHz. The nonlinear least-squares fitting routine employed was based on a Levenberg-Marquardt algorithm.[38] The adjustable parameters were $\Delta E_{\alpha\alpha}$, $\Delta E_{\alpha\beta}$, $\Delta E_{\beta\beta}$, the corresponding three Γ^{∞}, and Q. The parameters associated with the paramagnetic centers, kept fixed in the fits, were determined from T_1 below 250 K, i.e, in the regime where spin diffusion towards these centers predominates. In this regime, N_p and S_p are strongly correlated in the sense that they enter the expression for $T_1^{(p)}$, Eq. (12), in the combination $N_p[S_p(S_p+1)]^{1/4}$ only. We found

$$\tau_p=(1.7\pm 0.2)\times 10^{-9}\ \text{s},$$

without noticeable temperature dependence, and

$$N_p[S_p(S_p+1)]^{1/4}=(0.9\pm 0.2)\times 10^{24}\ \text{m}^{-3}.$$

The latter result would imply a concentration of, for instance, Nd^{3+} impurities ($S_p=\frac{3}{2}$) of approximately 40 ppm.

The result of the fit is shown in Fig. 6, and the output values of the parameters are given in Table II. As it appears, up to about 400 K all relaxation times are primarily dependent on $\Delta E_{\alpha\alpha}$ and $\Gamma_{\alpha\alpha}^{\infty}$, while above 400 K they are governed by $\Delta E_{\alpha\beta}$, Q, and $\Gamma_{\alpha\beta}^{\infty}$, and at the highest temperatures, to some extent by $\Delta E_{\beta\beta}$ and $\Gamma_{\beta\beta}^{\infty}$. The output parameters associated with different ionic motions are thus only weakly correlated, contrary to the Γ^{∞} and ΔE belonging to one another. The jump frequency $\Gamma_{\beta\beta}$ turned out to be considerably smaller than $\Gamma_{\beta\alpha}$ at all temperatures, and could therefore be determined with limited accuracy only. For this reason $\Delta E_{\beta\beta}$ was set equal to $\Delta E_{\alpha\beta}$ in the final fit, without introducing significant errors. A general conclusion of Fig. 6 is that there is satisfactory agreement, despite the assumptions made, between theory and experiment for all three relaxation times and over the entire range of temperatures considered. In particular, the maxima and minima of $T_{1\rho}$ and T_2 are well reproduced, except for minor departures of their positions; T_1, and its complicated frequency dependence, is excellently described except at the highest temperatures. The sizable

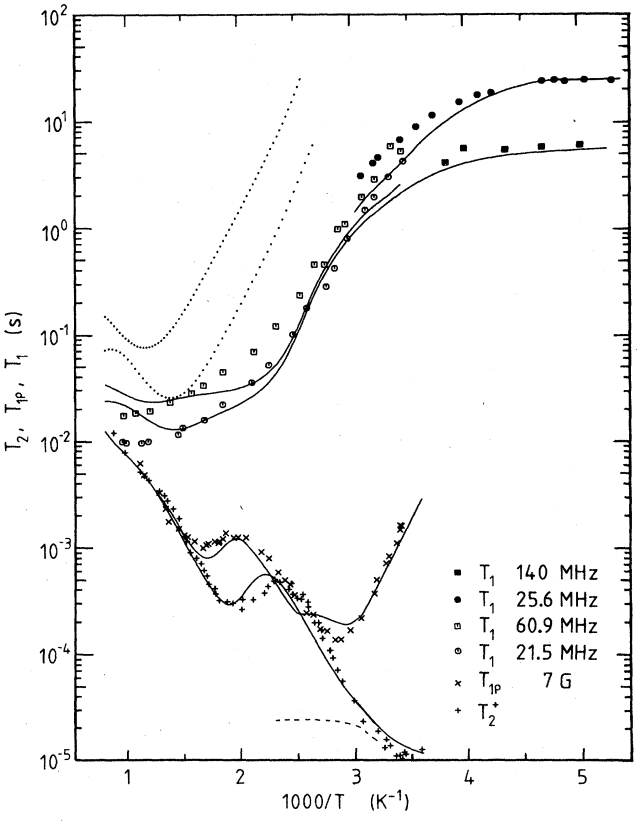

FIG. 6. Simultaneous fit of the theoretical expressions for T_2^{+}, $T_{1\rho}$, and T_1, Eqs. (14) with Eqs. (6), (17), and (18) inserted, to a selection of the data of Fig. 2. Dotted lines represent the contribution to T_1 of the fluorine-fluorine dipolar interaction. Dashed line denotes T_2^{-}.

TABLE II. Fit results of the model parameters. The indices α and β refer to the $F_{2,3}$ and F_1 sublattices, respectively.

Parameter	This work	Previous work
$\Delta E_{\alpha\alpha}$ (eV)	0.423±0.005	0.50[a]
		0.30[b]
		0.39±0.07[c]
		0.43±0.05[d]
		0.44±0.01[e]
		0.48±0.04[f]
		0.27[g]
$\Delta E_{\alpha\beta}$ (eV)	0.58 ±0.01	0.52[b]
		0.30[g]
$\Delta E_{\beta\beta}$ (eV)	0.58	0.60[g]
Q (eV)	0.119±0.005	
$\Gamma^{\infty}_{\alpha\alpha}$ (rad/s)	3.2×10^{14}	
$\Gamma^{\infty}_{\alpha\beta}$ (rad/s)	2.2×10^{13}	
$\Gamma^{\infty}_{\beta\beta}$ (rad/s)	5×10^{12}	
$[V_\alpha]\Gamma^{\infty}_{\alpha\alpha}$ (rad/s)	6.5×10^{10} [h]	7.5×10^{11} [b]
		3.7×10^{12} [d]
		7.5×10^{10} [g]
$[V_\beta]\Gamma^{\infty}_{\alpha\beta}$ (rad/s)	8.8×10^{9} [h]	5.0×10^{7} [g]
$[V_\beta]\Gamma^{\infty}_{\beta\beta}$ (rad/s)	2.0×10^{9} [h]	2.6×10^{11} [g]

[a]From NMR (line narrowing) (Ref. 8).
[b]From NMR (T_2) (Ref. 9).
[c]From NMR (T_1) (Ref. 10).
[d]From NMR (Ref. 11).
[e]From conductivity below 415 K (Ref. 12).
[f]From NMR ($T_{1\rho}$) (Ref. 14).
[g]From NMR (Ref. 16).
[h]Derived from Γ^{∞} and the extrinsic $[V_{\alpha,\beta}]$ from Ref. 28 extrapolated to infinite temperature.

frequency dependence of T_1 above 500 K is the result of the fluorine-fluorine dipolar interaction, which at these temperatures prevails over the relaxation to paramagnetic impurities. It should be noted that to disentangle the parameters combined fits to the relaxation times are necessary. For instance, it is not feasible to deduce $\Delta E_{\alpha\beta}$, $\Gamma^{\infty}_{\alpha\beta}$, and Q individually from T_2 alone, in contrast to simultaneous fitting with $T_{1\rho}$. Particularly, $\Delta E_{\alpha\beta}$ and Q are sensitive to $T_{1\rho}$ in relation to T_2 in the region between 400 and 600 K, i.e., where the exchange becomes manifest.

Since a nonzero Q constitutes a primary result of this investigation, we discuss the dependence of T_2 and $T_{1\rho}$ on Q in somewhat more detail. In Fig. 7, the best fit of $T_{1\rho}$ and T_2 with Q kept zero, i.e., with the assumption of a completely random distribution of vacancies over the sublattices, is compared with the fit yielding $Q=0.119$ eV. Marked departures, beyond the experimental uncertainties, are seen to occur between 400 and 600 K. A further argument against a vanishing Q is the strongly modified exchange-attempt frequency emerging from the $Q=0$ fit, $\Gamma^{\infty}_{\alpha\beta}=8\times10^{10}$ rad/s, compared with $\Gamma^{\infty}_{\alpha\beta}=2.2\times10^{13}$ rad/s of Table II. (The $Q=0$ value of $\Gamma^{\infty}_{\alpha\beta}$ here is compatible with the $Q=0$ result of $[V_\beta]\Gamma^{\infty}_{\alpha\beta}$ quoted in Ref. 16 upon account of the vacancy concentration.) The other parameters are only slightly affected. The resultant disparity between $\Gamma^{\infty}_{\alpha\alpha}$ and $\Gamma^{\infty}_{\alpha\beta}$, amounting to over 3 orders of magnitude, is obviously nonphysical in

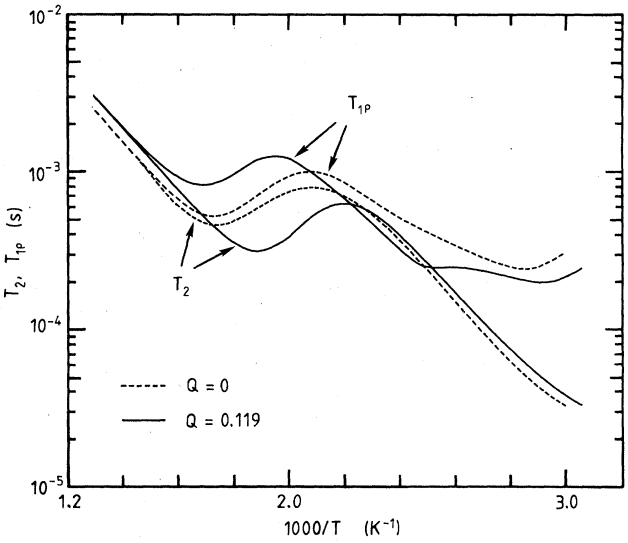

FIG. 7. Best fit for $Q=0$, compared with the fit of Fig. 6, showing the failure of the $Q=0$ fit to reproduce T_2 and $T_{1\rho}$ between $1000/T=1.8$ and 2.8 K^{-1}.

the case of equal concentrations of the vacancies on the sublattices. In an earlier paper,[24] an interpretation of $T_{1\rho}$ based on the implicit assumption $Q=0$ was also found to lead to nonphysical results. In this case the data were analyzed in terms of three additive BPP-like contributions, associated with the motions within the sublattices and an exchange. As it turned out, the minimum in $T_{1\rho}$ at 570 K could only be reproduced with too small a value for the second moment of the slow sublattice. By contrast, in the present model a finite Q has led to agreement for both $T_{1\rho}$ and T_2 using second moments derived from lattice summations (Table I). It is noted that the attempt frequencies deduced here are comparable with optical-phonon frequencies, and further that the result $\Delta E_{\alpha\alpha}=0.423\pm0.005$ eV agrees with the results $\Delta E=0.43$ eV (Ref. 11), 0.44±0.01 eV (Ref. 12), and 0.43±0.02 eV (Ref. 26) from conductivity experiments.

V. DISCUSSION

A crucial step in unraveling the ionic motion in LaF_3 has been to establish which fluorine sublattice carries the faster thermal motion. In the present investigation an unambiguous answer to this problem was found in the composite nature of the free-induction decays and the development of the associated time constants with temperature. The inequivalence of the F_1 and $F_{2,3}$ sublattices, as characterized by a finite Q, also offers an explanation as to why the analysis of Goldman and Shen[9] has led to a reversed identification of the two sublattices, implying, in our notation, $N^{\alpha}/N^{\beta}=2$ instead of $\frac{1}{2}$. The interpretation of their cross-relaxation experiment was essentially based on the assumption that the intensity ratio of the slow and fast components equals that of the ions on the sublattices at the temperature, where $N^{\alpha}a_{21}=N^{\beta}a_{12}=0$. As an inspection of the off-diagonal a's [cf. Eq. (3) with $\omega_1=0$] shows, this condition will not be ful-

filled if Q is significant relative to kT. Our results, on the other hand, confirm the conjecture by Goldman and Shen that the motion of the slower ions is dominated by exchange with vacancies on the sublattice carrying the faster motion.

Second, we consider the spin-lattice relaxation is LaF_3 doped with rare-earth ions. In the case of a Nd^{3+} dopant above 600 K, T_1 is first seen to rise with dopant concentration N_p in the range from 0.1 to 5 mol%, turning over to the usual decrease at higher concentrations.[10] From the preceding section it is apparent that in this temperature regime the spin-lattice relaxation arises at low N_p from the modulating nonsecular part of the fluorine-fluorine dipolar interaction. With increasing N_p, a growing fraction of the fluorine nuclei reside within the barrier radius b of an impurity. These nuclei have become unlike with the spins outside the barriers, yet do not effectively relax to the impurity. Under these conditions T_1 is increased by up to a factor of 2,[39] as observed.[10] At higher concentrations (5 mol% in case of Nd^{3+}), the relaxation towards the impurities remains efficient over the entire temperature range because the nucleus cannot diffuse away. The observation by Shen that T_1 at high N_p is independent of the temperature is indicative of a constant τ_p, like we have used in our calculations.

The preferential occupation of the $F_{2,3}$ sublattice by the vacancies, here introduced on grounds of NMR results, further is consequential in the understanding of a number of features of the conductivity σ as a function of the temperature. For LaF_3 a plot of $\log_{10}(\sigma T)$ vs $1/T$ is observed to exhibit a knee at 415 K.[12,26] Such a knee is also found in the solid solutions $La_{1-x}Ba_xF_{3-x}$,[26] as well as in a number of other materials with the tysonite structure, notably CeF_3.[23] The knee was initially ascribed to a classical changeover from a dissociation-governed regime of conductivity to a free-defect conduction mode at higher temperatures,[13,15,20] but evidence for a prevalence of free-vacancy motion already at low temperatures is found in the equality of the conductivity and NMR diffusion constants.[25,26] The result that free-vacancy motion governs the conduction was essentially confirmed by the behavior of the dielectric relaxation, which exhibits a space-charge peak near 120 K.[28] Although Q is relatively small compared to the migration energies, it severely affects the distribution of the vacancies over the two sublattices. At low temperatures the vacancies are virtually confined to the $F_{2,3}$, or α, sublattice, and it is not before 400 K that the effects of a population of the F_1, or β, sublattice become noticeable. Between 400 and 700 K the ratio $[V_\beta^{\cdot}]/[V_\alpha^{\cdot}]$ increases from $\frac{1}{30}$ to $\frac{1}{7}$, implying a reduction of the number of fast moving vacancies located on the α sublattice, and thereby a decrease of the slope of $\log_{10}(\sigma T)$ vs $1/T$. Although a decrease is indeed observed, it should be pointed out that the Q-invoked redistribution by itself would account for a reduction of σ relative to $\log_{10}(\sigma T)$ extrapolated from below 400 K by at most a factor of 3, overshooting the experimental σ by at least an order of magnitude.

Therefore, the conjecture is that the vacancies transferred to the slow β sublattice act to impede, via electrostatic repulsion, jumps within the fast α sublattice in so far as taking place near a vacancy-occupied β site, i.e., to locally lower the mobility of the conducting ions. Enhancement of the migration energy by defect-defect interaction has earlier been concluded to be realistic in the case of ZrO_2 by calculations based on the Debye-Hückel theory.[40] For concentrations similar to the ones here on the β sublattice a significant increment was found of the activation energies, linear with the concentration of repelling defects. In the present case of LaF_3, confirmation of this mechanism may be found in the conduction data when analyzed in terms of the Q introduced here. The β vacancies number, at any temperature in the extrinsic regime,

$$[V_\beta^{\cdot}]=3[V^{\cdot}]\exp(-Q/kT)/[1+2\exp(-Q/kT)] , \quad (19)$$

and it is assumed that these vacancies augment the migration energy of nearby α-α jumps by an amount $\Delta E'$. Expressing the associated ionic diffusive transport in terms of an effective diffusion in a homogeneous medium implies taking the average of $\Gamma_{\alpha\alpha}^{-1}$,[41] which converted to an activation energy amounts, for the purpose of conduction, to a modification of $\Delta E_{\alpha\alpha}$ in Eq. (17) to

$$\Delta E_{\alpha\alpha}^{(\sigma)}=\Delta E_{\alpha\alpha}+[V_\beta^{\cdot}]N^\beta/([V^{\cdot}]N^\alpha)\Delta E' . \quad (20)$$

When a finite measuring time is used, as is the case upon employing ac methods, the concentration $[V_\beta^{\cdot}]$ need, of course, be sufficiently large for the distance covered by the diffusion to exceed the separation of the β vacancies. For a numerical estimate for $\Delta E'$ in LaF_3, we have reanalyzed the ac-conductivity data points taken by Roos *et al.*[26] between 300 and 850 K down to 10^{-2} Hz. We use the Nernst-Einstein relation

$$\sigma T=N^\alpha e^2 D_\alpha^{(\sigma)}/k , \quad (21)$$

in which

$$D_\alpha^{(\sigma)}=\tfrac{1}{6}f\Gamma_{\alpha\alpha}^{(\sigma)}(T)a_{\text{F-F}}^2 ,$$

to obtain $\Gamma_{\alpha\alpha}^{(\sigma)}(T)$, and therefrom with Eq. (17) $\Delta E_{\alpha\alpha}^{(\sigma)}(T)$. Note that in Eq. (17) $[V_\alpha^{\cdot}]$ depends on the temperature according to $1/[1+2\exp(-Q/kT)]$. The resultant $\Delta E_{\alpha\alpha}^{(\sigma)}(T)$ are plotted in Fig. 8 as a function of $[V_\beta^{\cdot}]$ to verify Eq. (20). The result indeed is a straight line above $[V_\beta^{\cdot}]=5\times10^{-5}$, which is just at the temperature where the diffusion length has become of the order of the separation of the β vacancies. At this point, $D_\alpha^{(\sigma)}=4\times10^{-13}m^2/\text{s}$, while the maximum drift time is $t=1/\pi\omega=30$ s, corresponding to a diffusion length of $(2Dt)^{1/2}=2\times10^4$ lattice units, consistent with $[V_\beta^{\cdot}]$ at the threshold. Figure 8 thus reflects that the redistribution over the sublattices according to Q provides an explanation of the conductivity knee. Below the threshold we have $\Delta E_{\alpha\alpha}=0.445$ eV for unhindered α motion perpendicular to the c axis, and similarly $\Delta E_{\alpha\alpha}=0.415$ eV parallel to the c axis, in accord with the NMR results, while from the slope $\Delta E'=0.5$ eV for conduction parallel to the c axis, and $\Delta E'=0.45$ eV for conduction perpendicular to the c axis. Therefore, LaF_3 is an example of a ionic conductor in which the effects of defect-defect interaction vary with the temperature. This stands in contrast to

what is found in ionic conductors prepared by doping, like $Ba_{1-x}U_xF_{2+2x}$, in which the defect concentrations in the extrinsic regime depend on the solute content only.

Another mechanism, based on crystallographic arguments, to explain the knee in the conductivity has recently been proposed by Franceschetti and Shipe,[29] and we comment on it in some detail in relation to our findings. Their treatment of LaF_3 has been cast in terms of an equivalent circuit of layers carrying a mutual polarization. The anion vacancies are assumed to be situated on inequivalent lattice planes A and B perpendicular to the applied electric field. In the case the field is parallel to the c axis, the stacking of the planes is $\ldots BBABBA\ldots$. The interplanar jump probabilities of the vacancies Γ_{AB}, Γ_{BA}, and Γ_{BB}, in a notation equivalent to ours, give rise to an apparent bulk resistance at high frequencies

$$\sigma^{-1}=\frac{kT}{e^2[V_F^{\cdot}]}\left[\frac{2+\Gamma_{BA}/\Gamma_{AB}}{c^2\Gamma_{BB}+2d^2\Gamma_{BA}}\right], \tag{22}$$

with c the separation between B planes and d between A and B planes. Equation (22) represents a knee in the conductivity parallel to the c axis for appropriately chosen Γ's. Although the outcome of the model is of general interest in that it provides a phenomenological description of the ionic conductivity in materials with inequivalent sites, its application to LaF_3 is questionable. A definitive argument against the model of polarized planes is supplied by the NMR results, which evidence a fast motion by jumps between the $F_{2,3}$ sites. This motion provides a connected path for the vacancies through the entire lattice, and inhibits the development of polarization on the scale of lattice displacements. Second, the conductivity in LaF_3 does not exhibit any anisotropy at temperatures above the knee, whereas the sequence of planes would vary from one direction of the field to another. In particular, if the field is directed perpendicular to the planes spanned by the c axis and La-$F_{2,3}$ displacements, all lattice planes would be equivalent, removing any effects of polarization. In fact, Eq. (22) would return to the Nernst-Einstein relation, Eq. (21), with a single Γ, contrary to experiment.

We finally turn to the intrinsic regime, which becomes manifest in the conductivity above 715 K,[26] and in the NMR above 1000 K (Fig. 2). The low value of the apparent migration energy derived from the conductivity, $\Delta E_m^{(\sigma)}=0.26$ eV, makes it plausible why the onset of the intrinsic regime is not observed in the NMR until high temperatures. The conductivity predominantly probes the motion of the fast α vacancies, whereas T_2 and $T_{1\rho}$ are at these temperatures particularly sensitive to the relatively slow exchange between the β and α sublattices. The migration energy of the $\beta\rightarrow\alpha$ jump as measured by NMR equals $\Delta E_m^{(\mathrm{NMR})}=\Delta E_{\alpha\beta}+\frac{1}{2}Q=0.64$ eV. For both the conductivity and the NMR, the transition from the extrinsic regime to the intrinsic regime is determined, as regards the temperature-dependent part, by

$$\exp[(\Delta E_m+\Delta E_f/4)/kT]\ ,$$

where ΔE_f is the formation energy for a Schottky quartet. Upon taking $\Delta E_f=2.3$ eV,[26] it then follows from the transition temperature of the conductivity that the NMR will not see intrinsic behavior below 1040 K.

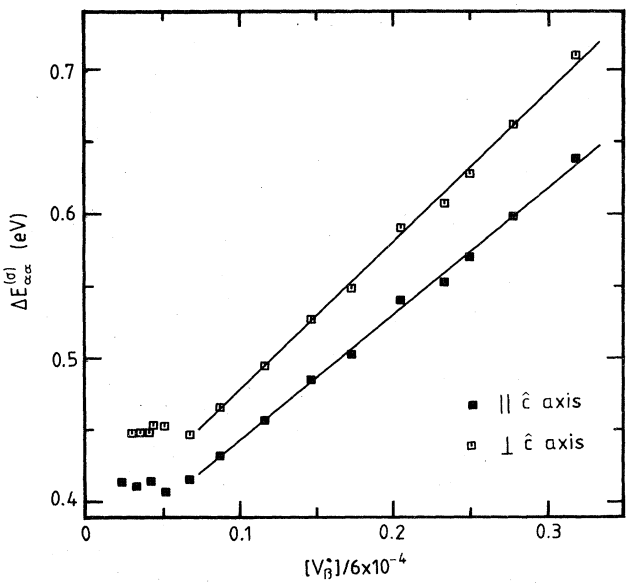

FIG. 8. Activation energy $\Delta E_{\alpha\alpha}^{(\sigma)}(T)$ as a function of the vacancy concentration on the β sublattice. The data points are from Ref. 26, reworked to $\Delta E_{\alpha\alpha}^{(\sigma)}$ according to Eqs. (20) and (21).

VI. CONCLUSIONS

We have demonstrated that the ionic motion as observed by the various decay times of NMR over a wide range of temperatures can be accounted for by a two-sublattice theory based on relaxation by dipolar interactions and residual paramagnetic centers. The frequencies of the jumps within the sublattices as well as those between the sublattices may be taken to be described, as proposed before, by single activation energies. A primary result of the present work is that allowance should be made for an energy difference, which is substantial relative to kT, between fluorine ions residing on F_1 and $F_{2,3}$ sites. The F_1 sites are favored, and the ionic conductivity is governed by the thermal motion of vacancies over the $F_{2,3}$ sublattice. The activation energy found for the motion within the $F_{2,3}$ sublattice equals the one derived from the conductivity below the point where the F_1 sublattice becomes significantly populated by vacancies (415 K). The knee observed in the conductivity above this point is accounted for by the defect-defect interaction with vacancies transferred to the F_1 sublattice at higher temperatures. The conclusions arrived at here in LaF_3, in particular on the distribution of the vacancies, also have a bearing on the ionic motion in other tysonite-structured ionic con-

ductors, notably the solid solutions $La_{1-x}Ba_xF_{3-x}$. It is finally worth noting that the activation energies, the jump frequencies, and the energy difference Q are accessible to confirmation by molecular-dynamics calculations when applied to the tysonite-type ionic conductors. In particular, the transfer of the vacancies to the slow sublattice is verifiable by a computer simulation. In spite of the intricate crystal structure of LaF_3, sufficient physical information is available to perform such a study with reliable interionic potentials.

ACKNOWLEDGMENTS

The authors are indebted to Professor J. H. Strange for sending a copy of his work done in collaboration with Dr. G. A. Jaroszkiewicz prior to publication. They further acknowledge many useful discussions with Professor J. Schoonman. The work was financially supported by the Netherlands Foundations Fundamenteel Onderzoek der Materie (FOM) and Zuiver Wetenschappelijk Onderzoek (ZWO).

[1]D. R. Figueroa, A. V. Chadwick, and J. H. Strange, J. Phys. C **11**, 55 (1978).
[2]R. E. Gordon and J. H. Strange, J. Phys. C **11**, 3213 (1978).
[3]R. W. Bonne and J. Schoonman, J. Electrochem. Soc. **124**, 28 (1977).
[4]M. Mansmann, Z. Anorg. Allg. Chem. **331**, 98 (1964).
[5]K. Schlyter, Arkiv. Kemi **5**, 73 (1952).
[6]K. Lee and A. Sher, Phys. Rev. Lett. **14**, 1027 (1965).
[7]A. G. Lundin and S. P. Gabuda, Fiz. Tverd. Tela (Leningrad) **8**, 1889 (1966) [Sov. Phys.—Solid State **8**, 1495 (1966)].
[8]A. G. Lundin, S. P. Gabuda, and A. I. Lifshits, Fiz. Tverd. Tela (Leningrad) **9**, 357 (1967) [Sov. Phys.—Solid State **9**, 273 (1967)].
[9]M. Goldman and L. Shen, Phys. Rev. **144**, 321 (1966).
[10]L. Shen, Phys. Rev. **172**, 259 (1968).
[11]A. Sher, R. Solomon, K. Lee, and M. W. Muller, Phys. Rev. **144**, 593 (1966).
[12]J. Schoonman, G. Oversluizen, and K. E. D. Wapenaar, Solid State Ionics **1**, 211 (1980).
[13]J. R. Igel, M. C. Wintersgill, J. J. Fontanella, A. V. Chadwick, C. G. Andeen, and V. E. Bean, J. Phys. C **15**, 7215 (1982).
[14]E. Ildstad, I. Svare, and T. A. Fjeldly, Phys. Status Solidi A **43**, K65 (1977).
[15]A. V. Chadwick, D. S. Hope, G. A. Jaroszkiewicz, and J. H. Strange, in *Fast Ion Transport in Solids*, edited by P. Vashista, J. N. Mundy, and G. K. Shenoy (Elsevier, Amsterdam, 1979), p. 683.
[16]G. A. Jaroszkiewicz and J. H. Strange, J. Phys. (Paris) Colloq. C6-246 (1980).
[17]G. A. Jaroszkiewicz and J. H. Strange, J. Phy. C **18**, 2331 (1985). We have rederived the relevant equations.
[18]B. Maximov and H. Schulz (unpublished).
[19]A. E. Aliev, V. L. Komashnya, L. N. Fershtat, and P. K. Khabibullaev, Fiz. Tverd. Tela (Leningrad) **25**, 2818 (1983) [Sov. Phys.—Solid State **25**, 1627 (1983)].
[20]A. Kessler, R. Hüger, and I. V. Murin, Mater. Res. Bull. **16**, 1185 (1981).
[21]K. Lee, Solid State Commun. **7**, 367 (1969).
[22]F. C. Case and P. P. Mahendroo, J. Phys. Chem. Solids **42**, 385 (1981).
[23]T. Takahashi, H. Iwahara, and T. Ishikawa, J. Electrochem. Soc. **124**, 280 (1977).
[24]A. F. Aalders, A. Polman, A. F. M. Arts, and H. W. de Wijn, Solid State Ionics **9**, 539 (1983).
[25]A. Roos, A. F. Aalders, J. Schoonman, A. F. M. Arts, and H. W. de Wijn, Solid State Ionics **9**, 571 (1983).
[26]A. Roos, F. C. M. van de Pol, R. Keim, and J. Schoonman, Solid State Ionics **13**, 191 (1984).
[27]A. Roos and J. Schoonman, Solid State Ionics **13**, 205 (1984).
[28]A. Roos, M. Buijs, K. E. D. Wapenaar, and J. Schoonman, J. Phys. Chem. Solids **46**, 655 (1985).
[29]D. R. Franceschetti and P. C. Shipe, Solid State Ionics **11**, 285 (1984).
[30]H. E. Rorschach, Jr., Physica (Utrecht) **30**, 38 (1964).
[31]P. M. Richards, Phys. Rev. B **18**, 6358 (1978).
[32]A. Roos, Mater. Res. Bull. **18**, 405 (1983).
[33]L. Gmelin, *Handbuch der Anorganischen Chemie*, 8th ed. (Springer, Berlin, 1976), Teil 3, p. 99.
[34]D. Wolf, J. Magn. Reson. **17**, 1 (1975).
[35]D. R. Figueroa, J. H. Strange, and D. Wolf, Phys. Rev. B **19**, 148 (1979).
[36]S. P. Vernon, P. Thayamballi, R. D. Hogg, D. Hone, and V. Jaccarino, Phys. Rev. B **24**, 3756 (1981).
[37]F. A. Kröger, *The Chemistry of Imperfect Crystals*, 2nd ed. (North-Holland, Amsterdam, 1974), Vol. 2, p. 7.
[38]D. W. Marquardt, J. Appl. Math. **11**, 431 (1963).
[39]A. Abragam, *The Principles of Nuclear Magnetism* (Oxford University Press, Oxford, 1961), p. 295.
[40]H. Schmalzried, Z. Phys. Chem. (Wiesbaden) **105**, 47 (1977).
[41]This procedure is rigorous in one dimension for symmetric potential barriers; B. Derrida, J. Stat. Phys. **31**, 433 (1983).